iScience

CellPress OPEN ACCESS

Article

Developing a thermally stable Co/Ce-Sn catalyst via adding Sn for soot and CO oxidation

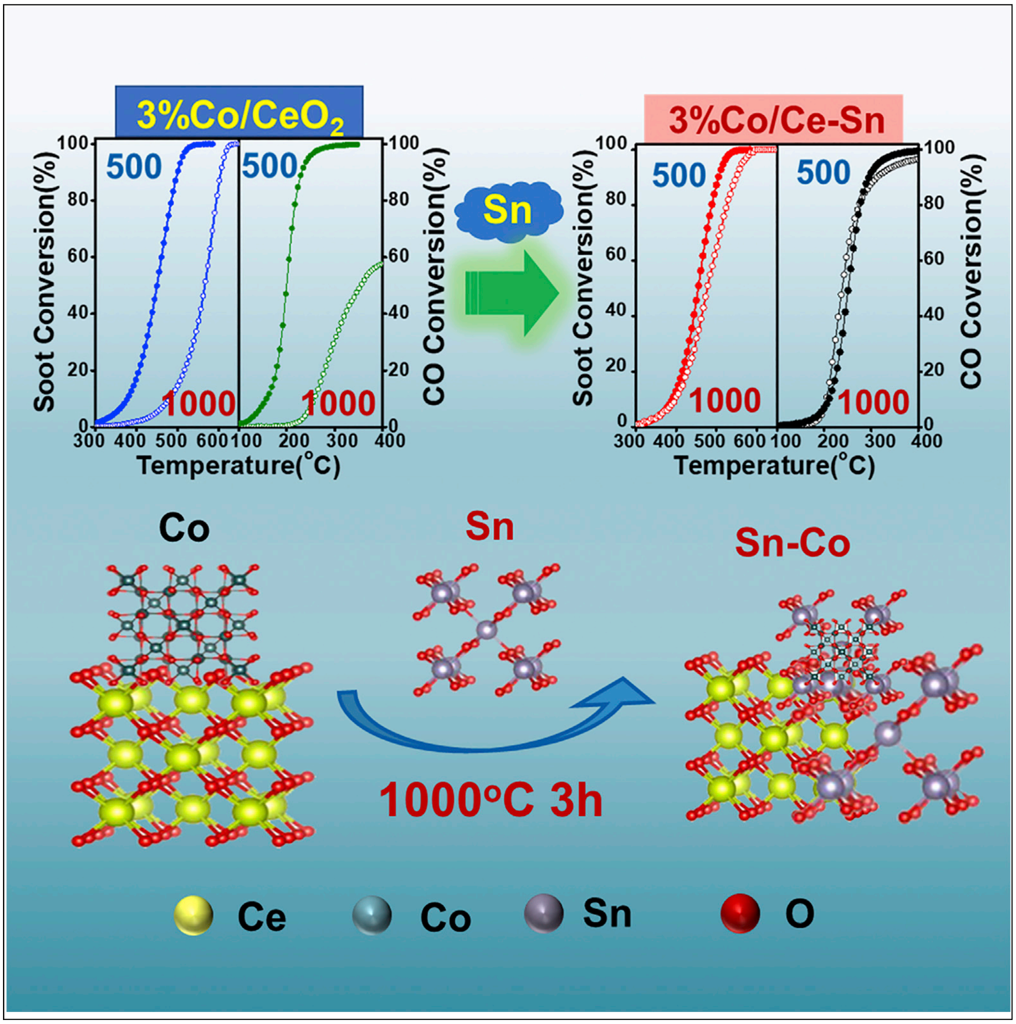

Meng Wang, Yan Zhang, Wenpo Shan, Yunbo Yu, Jingjing Liu, Hong He

yzhang3@iue.ac.cn (Y.Z.)
wpshan@iue.ac.cn (W.S.)
honghe@rcees.ac.cn (H.H.)

Highlights

The developed 3%Co/Ce-Sn catalyst processes extraordinary thermal stability

The Sn species could restrain the aggregation of Co active component

The Sn-Co solid solution plays a key role in improving the thermal stability

The 3%Co/Ce-Sn catalyst exhibited perfect and stable resistance to H_2O and SO_2

Wang et al., iScience *25*, 104103
April 15, 2022
https://doi.org/10.1016/j.isci.2022.104103

iScience

CellPress
OPEN ACCESS

Article

Developing a thermally stable Co/Ce-Sn catalyst via adding Sn for soot and CO oxidation

Meng Wang,[1,2] Yan Zhang,[1,2,*] Wenpo Shan,[1,2,5,*] Yunbo Yu,[1,3,4] Jingjing Liu,[3] and Hong He[1,3,4,*]

SUMMARY

The thermal stability of the catalysts is of particular importance but still a big challenge for working under harsh conditions at high temperature. In this study, we report a strategy to improve the thermal stability of the ceria-based catalyst via introducing Sn. XRD, Rietveld refinement, and other characterizations results indicated that the formation of Sn-Co solid solution plays a key role in the thermal stability of the catalyst. The developed ternary 3%Co/$Ce_{0.5}Sn_{0.5}O_2$ catalyst not only exhibits outstanding thermal stability and resistance to SO_2 and H_2O for soot oxidation from diesel vehicle exhaust but also remains extraordinary thermal stability for CO oxidation. Remarkably, even after thermal aging at 1000°C, it still possessed high catalytic activity similar to that of the fresh catalyst.

INTRODUCTION

With the rapid development of catalytic science and technology, catalytic materials are applied widely in environment, devices, biomedicine, and so on. During these applications, the catalytic materials are placed under all kinds of harsh conditions, such as high temperature environment and so forth. Therefore, thermal stability is often a crucial feature determining the practical application of catalysts (Xu et al., 2018; Yang et al., 2019; Liu et al., 2018; Yan et al., 2020; Wang et al., 2020; Zhang et al., 2017).

To improve the thermal stability of the catalysts, great efforts have been devoted. For example, Xu et al. reported a novel entropy-driven strategy to stabilize Pd single atom on the high-entropy fluorite oxides, which exhibited excellent resistance to thermal and hydrothermal degradation (Xu et al., 2020). In addition, modifying with dopants is also applied to resist the sintering of active components. For the three-way catalysts (TWCs) applied in the gasoline engine aftertreatment, Zr is added into CeO_2 to resist the aggregation of active components (Pt, Pd, and Rh) and stabilize the ability of oxygen storage (Farrauto et al., 2019; Monte et al., 2004). Compared with gasoline engines, diesel engines are widely used owing to high fuel efficiency, durability, and excellent dynamic performance. Yet, the development of aftertreatment catalysts with excellent thermal stability still remains a huge challenge in diesel emission control. When the DPF is regenerated to remove the collected particulate matter, the peak temperature inside the DPF can even reach 1000°C (Guo and Zhang, 2007; Yu et al., 2013a, 2013b). Thus, not only high catalytic activity but also good thermal stability is essential for the aftertreatment catalysts, such as CO oxidation and soot oxidation catalysts. For instance, a MnO_x-CeO_2-Al_2O_3 catalyst for soot oxidation reported by Wu et al. (2011) exhibited good thermal stability, due to the introduction of stabilized Al_2O_3 and its maximum soot oxidation only shifted upward by 53°C after aging treatment at 800°C for 20 h. In addition, Zr doping has been reported to be able to improve the thermal stability of CeO_2 calcined at 1000°C, but the T_{50} of soot oxidation for the obtained Ce-Zr mixed oxide was only about 20°C lower than that without a catalyst (Atribak et al., 2008).

Above all, the development of the catalysts with excellent thermal stability is still urgently needed for industrial catalytic application, especially for those involving high-temperature environment. However, the previously reported aftertreatment catalysts usually cannot hold their activity after thermal aging even at 800°C. Therefore, the thermal stability of this type of catalysts remains a formidable challenge.

In our previous development of the catalysts for selective catalytic reduction of NO_x with NH_3 (NH_3-SCR), it was found that SnO_2 can remarkably promote a Ce-W mixed oxides catalyst for sintering resistance at high temperatures, which was related to the preservation of highly dispersed Ce-W species induced by Sn

[1]Center for Excellence in Regional Atmospheric Environment, Institute of Urban Environment, Chinese Academy of Sciences, Xiamen 361021, China

[2]Zhejiang Key Laboratory of Urban Environmental Processes and Pollution Control, Ningbo Urban Environment Observation and Research Station, Institute of Urban Environment, Chinese Academy of Sciences, Ningbo 315800, China

[3]State Key Joint Laboratory of Environment Simulation and Pollution Control, Research Center for Eco-Environmental Sciences, Chinese Academy of Sciences, Beijing 100085, China

[4]University of Chinese Academy of Sciences, Beijing 100049, China

[5]Lead contact

*Correspondence:
yzhang3@iue.ac.cn (Y.Z.),
wpshan@iue.ac.cn (W.S.),
honghe@rcees.ac.cn (H.H.)

https://doi.org/10.1016/j.isci.2022.104103

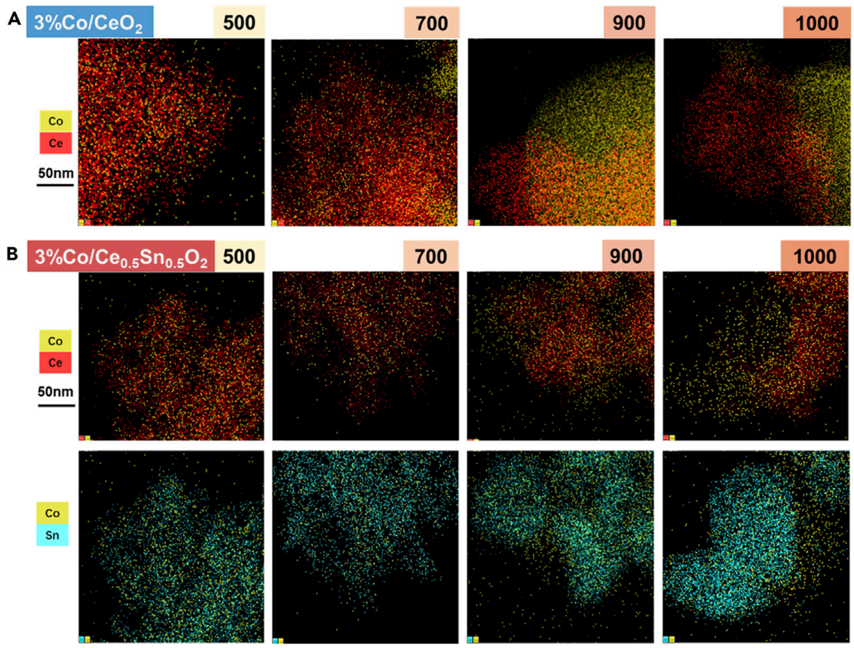

Figure 1. Element distributions measurements

EDS elemental mapping images of the (A) $3\%Co/CeO_2$ and (B) $3\%Co/Ce_{0.5}Sn_{0.5}O_2$ catalysts at different aging temperatures.

(Liu et al., 2021). In addition, it was reported that doping Sn could also improve the oxygen storage capacity (OSC) of CeO_2-based materials because the reversible $Sn^{4+} \leftrightarrows Sn^{2+}$ redox process involves two electrons transfer (Liu et al., 2015; Mukherjee et al., 2018). For instance, Chang et al. found Sn-modified MnO_x-CeO_2 catalysts presented nearly 100% NO_x conversion at 110°C–230°C, which is associated with that doping of Sn can promote the formation of oxygen vacancies and facilitate NO oxidation to NO_2 (Chang et al., 2013). In Sasikala's work, it was found that a Ce-Sn mixed oxide exhibited better catalytic activity for CO oxidation reaction as comparing with their pure oxides due to a synergetic effect between Ce and Sn (Sasikala et al., 2001). Therefore, Sn is very attractive for the development of the catalysts with excellent activity and thermal stability. Herein, we report a facile strategy to develop outstanding thermally stable non-noble catalyst via introducing Sn. A series of $Ce_{1-x}Sn_xO_2$ supports with different Ce/Sn molar ratios were prepared by a co-precipitation method, and then Co was loaded on the optimal $Ce_{0.5}Sn_{0.5}O_2$ support (Figure S1) by the impregnation method. All catalysts were calcined at 700°C for 3 h. Meanwhile, the optimal $3\%Co/Ce_{0.5}Sn_{0.5}O_2$ catalyst (Figure S2) was calcined at 500, 700, 900, and 1000°C for 3 h for the thermal stability tests.

RESULTS AND DISCUSSION

Figure 1 displays a series of elemental mapping images of the catalysts aging at different temperatures. As shown in Figure 1A, with the increase of aging temperature, Co_3O_4 phase over the $3\%Co/CeO_2$ catalyst was aggregated, indicating that aging treatment has a negative effect on the $3\%Co/CeO_2$. Yet, the introduction of Sn could restrain the aggregation of Co_3O_4, as confirmed by the elemental mapping and TEM imagines in Figures 1B, S3, and S4. In addition, the surface areas values of the as-prepared catalysts are presented in Table S1. The results showed that the specific surface areas of all the catalysts decreased with the increase of aging temperatures. Yet, after thermal aging at high temperatures (900 and 1000°C), the developed ternary $3\%Co/Ce_{0.5}Sn_{0.5}O_2$ catalyst exhibited larger surface area than $3\%Co/CeO_2$, indicating that the addition of Sn had a positive effect on the specific surface area.

The crystal structures of the $3\%Co/CeO_2$ and $3\%Co/Ce_{0.5}Sn_{0.5}O_2$ catalysts subjected to different aging temperatures were examined by XRD (Figures 2, S5, and S6). For the $3\%Co/CeO_2$ catalyst calcined at 500°C, it exhibited the structures of cubic fluorite CeO_2 (PDF#43-1002), and no peaks of any Co species were observed. Figure 2A shows that there is no shift for the peak of (220) crystal face of CeO_2 in the 3%

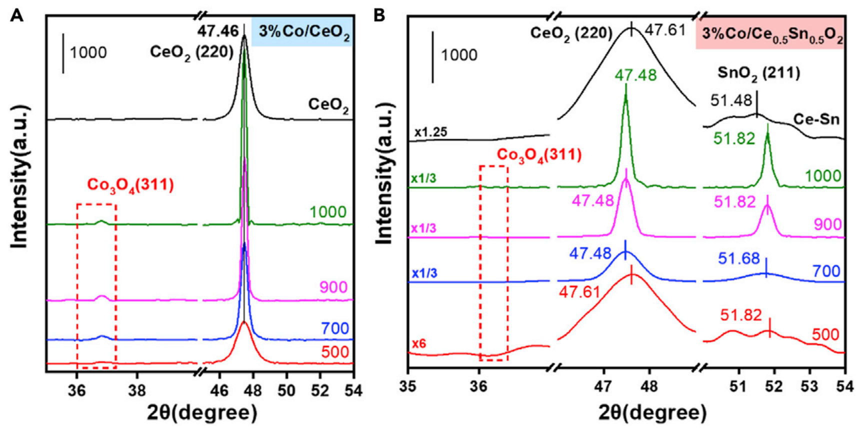

Figure 2. XRD analysis

XRD patterns of (A) 3%Co/CeO_2 and (B) 3%Co/$Ce_{0.5}Sn_{0.5}O_2$ catalysts at different aging temperatures.

Co/CeO_2 catalyst, in comparation with the pure CeO_2 sample. These results indicated that Co species were highly dispersed on the CeO_2 surface rather than existing as Ce-Co solid solutions (He et al., 2018; Venkataswamy et al., 2015). Moreover, when the aging temperature increased to 700, 900, and 1000°C, cubic Co_3O_4 phase was detected, and the crystallite size of Co_3O_4 calculated by the Scherrer formula (in Table S1) also increased gradually for the 3%Co/CeO_2 catalyst (shown in Figure 2A), which can be attributed to the sintering of the active Co component.

Amazingly, as presented in Figures S2B and S5B, no peaks of the Co_3O_4 phase were found for the 3%Co/$Ce_{0.5}Sn_{0.5}O_2$ catalyst, even after thermal aging at 1000°C. The patterns of 3%Co/$Ce_{0.5}Sn_{0.5}O_2$ catalyst calcined at 700°C (shown in Figure S6A) mainly showed the typical peaks of CeO_2 (PDF#43-1002) and SnO_2 (PDF#41-1445). Figures S6B and S6C depict the enlarged drawing of XRD patterns, corresponding to the (220) facet of CeO_2 and the (211) facet of SnO_2 in the $Ce_{0.5}Sn_{0.5}O_2$ and 3%Co/$Ce_{0.5}Sn_{0.5}O_2$ catalysts. With the addition of Co, the peak of the (211) facet of SnO_2 shifted to higher diffraction angle, indicating the formation of Sn-Co solid solution. Yet, the peak of the (220) facet of CeO_2 shifted to lower diffraction angle, which could be due to the occurrence of Sn phase segregation from Ce-Sn solid solution (see Figures S7 and S8A in supplemental information). Figure 2B showed that the peak of the (220) facet of CeO_2 in aged 3%Co/$Ce_{0.5}Sn_{0.5}O_2$ shifted to lower diffraction, while the peak of the (211) facet of SnO_2 still located at higher diffraction angle than the $Ce_{0.5}Sn_{0.5}O_2$ catalyst, which suggested the still existence of Sn-Co solid solution. In addition, a new phase of Co_2SnO_4 was detected for the 3%Co/$Ce_{0.5}Sn_{0.5}O_2$ catalyst aging at 900°C and 1000°C (Figure S9), which further indicated that Co preferred to interact with Sn species.

Rietveld refinement was performed using Fullprof Suite to obtain precise lattice parameters (Rodriguez-Carvajal, 1993), and the results are described in Figures 3 and S8. Figure 3A shows the refined XRD patterns of the 3%Co/CeO_2 catalysts aging at different temperature and the a, b, and c values of CeO_2 were almost equal to the pure CeO_2 sample (shown in Figure S8A), which further revealed that Co_3O_4 ought to exist mainly as dispersed crystallites rather than Ce-Co solid solutions. As shown in Figure S8B, the c value of SnO_2 in 3%Co/$Ce_{0.5}Sn_{0.5}O_2$ catalyst was smaller than that in $Ce_{0.5}Sn_{0.5}O_2$, while the a, b, and c values of CeO_2 were slightly larger than those of the $Ce_{0.5}Sn_{0.5}O_2$ catalyst. These results indicated that the Co was doped to SnO_2 instead of CeO_2 lattice. Thus, the Sn-Co solid solution formed through the replacement of Sn^{4+} (0.071 nm) by smaller Co^{3+} (0.061 nm). The lattice parameters of CeO_2, SnO_2, and Co_2SnO_4 in the aged 3%Co/$Ce_{0.5}Sn_{0.5}O_2$ catalysts obtained by Rietveld refinement are shown in Figure 3B. The c values of SnO_2 in the aged 3%Co/$Ce_{0.5}Sn_{0.5}O_2$ are still smaller than that in the $Ce_{0.5}Sn_{0.5}O_2$ catalyst (shown in Figure S8A). It suggested that Sn-Co solid solution was not destroyed by high-temperature treatment. Additionally, the Co_2SnO_4 phase was also identified by Rietveld refinement, and the results are shown in Figure S8C. The above results indicated that the introduction of Sn could improve the thermal stability via the formation of Sn-Co solid solution to restrain the aggregation of Co_3O_4.

X-ray photoelectron spectroscopy (XPS) technology was employed to explore the surficial properties of the as-prepared catalysts, and the results are shown in Figures 4 and S10. As the aging temperature increases,

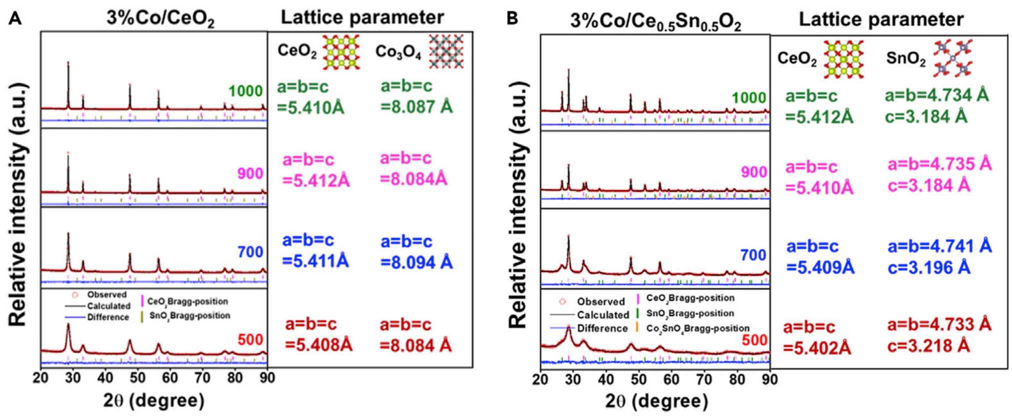

Figure 3. Rietveld refinement of XRD patterns

Rietveld refined XRD patterns of the (A) 3%Co/CeO_2 and (B) 3%Co/$Ce_{0.5}Sn_{0.5}O_2$ catalysts at different aging temperatures.

the proportion of Co^{2+}/Co^{3+} and Ce^{3+}/Ce^{4+} on the surface of the 3%Co/CeO_2 catalyst gradually decreased. As is well known, the higher the Ce^{3+} and Co^{2+} concentration in these samples, the more oxygen defects are generated (Zhao et al., 2019; Liu et al., 2009). Therefore, the surface oxygen defects associating with the Co^{2+} and Ce^{3+} of the 3%Co/CeO_2 catalyst gradually disappeared, with the increase of aging temperature (Zhao et al., 2019; Cui et al., 2020; Wang et al., 2018; Ren et al., 2019). Figure S10 showed that the O 1s spectra of all catalysts can be deconvoluted into two kinds of O species, with the peak at higher binding energy being attributed to the surface oxygen species (O_α) and the peak at lower binding energy being ascribed to the lattice oxygen species (O_β) (Xu et al., 2020; Ren et al., 2019; Sellers-Anton et al., 2020). The ratio of O_α/O_β over the 3%Co/CeO_2 catalyst decreased obviously with the increase of aging temperature. Yet, after introducing the Sn, the amount of surface Co^{2+}, Ce^{3+}, and O_α for the catalysts aged at different temperatures did not change significantly. In addition, the results of H_2-TPR (Figure S11) showed that with the addition of Sn, the H_2 consumption significantly increased, which indicated that Sn addition is beneficial to the formation of active oxygen species.

According to the above characterization results, the addition of Sn can protect the active Co component of the 3%Co/$Ce_{0.5}Sn_{0.5}O_2$ catalyst via the formation of Sn-Co solid solution, and the aged catalysts exhibited similar amounts of surface O_α with the fresh one. Surface-active oxygen species play a significant role in

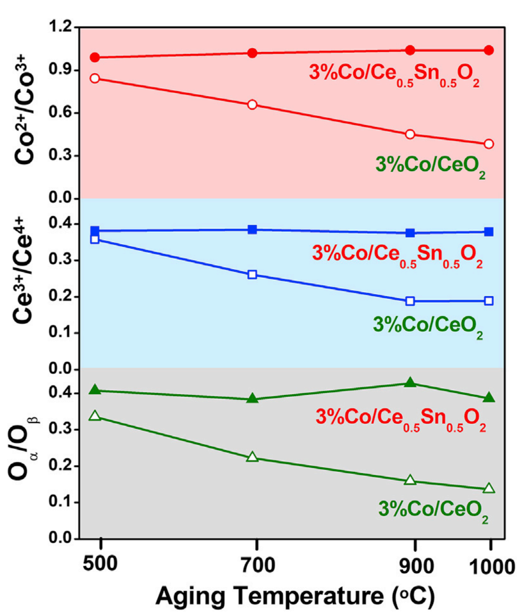

Figure 4. Analysis of the surficial properties

The ratios of Co^{2+}/Co^{3+}, Ce^{3+}/Ce^{4+}, and O_α/O_β ratios of as-prepared catalysts at different aging temperatures.

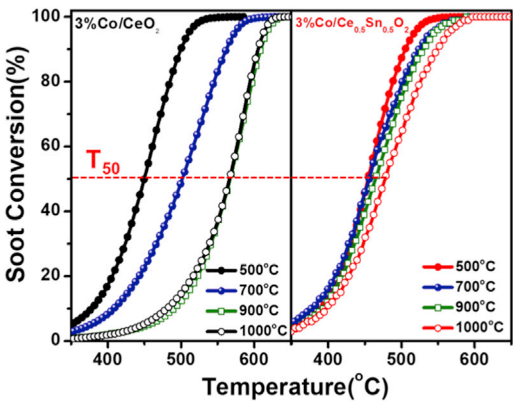

Figure 5. Soot conversion of the catalysts with different aging temperatures during temperature-programmed oxidation of soot

Reaction conditions: 0.1% NO and 10% O_2 balanced by N_2, under loose contact mode, GHSV = 300,000 mL $g^{-1}\cdot h^{-1}$, and heating rate = 10°C/min.

many heterogeneous catalytic reactions, including solid-solid-gas and gas-gas-solid reactions. For solid-solid-gas reaction, soot oxidation is a typical represent and the catalyst would undergo high-temperature oxidation process in the actual application. Thus, we tested the catalytic performance of soot oxidation for the catalysts to verify whether the catalyst with Sn introduction possess stable catalytic activity. As shown in Figure 5, the 3%Co/$Ce_{0.5}Sn_{0.5}O_2$ catalyst indeed exhibited extraordinarily thermal stability, with high soot conversion activity still maintaining even after aging at 1000°C, indicating its high resistance to thermal shock. For a comparative study, we tested the soot oxidation performances of the 3%Co/CeO_2 catalyst aged at different temperatures. The results showed that the soot combustion temperature over the 3% Co/CeO_2 catalyst increased sharply with the increase of aging temperature, while that over 3%Co/ $Ce_{0.5}Sn_{0.5}O_2$ did not show a noticeable increase after aging at different temperatures from 500°C to 1000°C. In addition, even after 1000°C aging, the CO_2 selectivity of the 3%Co/$Ce_{0.5}Sn_{0.5}O_2$ catalyst was still nearly 100%, while that of the 3%Co/CeO_2 catalyst decreased remarkably (Figure S12). These results indicate that Sn plays a key role in the thermal stability of the 3%Co/$Ce_{0.5}Sn_{0.5}O_2$ catalyst. As we all know, the presence of sulfur compounds in diesel fuels and water vapor in the exhaust gas is almost unavoidable. Therefore, tolerance of the SO_2 and H_2O in diesel exhaust also plays an important role in the application of a soot oxidation catalyst. Figures S13 and S14 showed that the 3%Co/$Ce_{0.5}Sn_{0.5}O_2$ catalyst possess high and stable resistance to H_2O and SO_2, which was of extraordinary importance for its practical application.

Moreover, there are also many gas-gas-solid reactions, in which the catalysts could be exposed to high-temperature conditions, such as catalytic elimination of emissions including CO, NO, HC, and so on from internal combustion engines. Therefore, CO-TPO experiment was also applied to further investigate whether the catalyst with doping Sn exhibited outstanding stability for CO oxidation, and the results are shown in Figure S15. It was found that the activity of 3%Co/CeO_2 decreased gradually with the aging temperature increasing from 500°C to 1000°C. Yet, the 3%Co/$Ce_{0.5}Sn_{0.5}O_2$ catalyst exhibited stable activity for CO oxidation, even after 1000°C aging (Figure S15B), which further confirmed that the introduction of Sn is the key to improve the stability of the catalyst.

Conclusion

In summary, we developed an extraordinary 3%Co/$Ce_{0.5}Sn_{0.5}O_2$ catalyst with outstanding thermal stability. The characterization results indicated that the introduction of Sn species induced the formation of Sn-Co solid solution to restrain the aggregation of the Co active component. Moreover, the results of soot and CO oxidations further illustrate the addition of Sn can remarkably improve the stability of the 3%Co/ CeO_2 catalyst. This study offers an efficient strategy toward developing the catalyst with outstanding thermal stability. Further optimization of this catalyst and investigation of the reaction mechanism are underway.

Limitations of the study

In this work, it provides a new and efficient strategy toward developing the catalyst with excellent thermal stability. For the analysis of surficial properties of the as-prepared catalysts, only XPS was used. Based on previous studies, the Co 2p spectra were deconvoluted into Co $^{2+}$ and Co^{3+}, and the O 1s spectra were deconvoluted into surface oxygen species (O_α) and lattice oxygen species (O_β). More evidence of surficial properties, such as *in situ* XPS, *in situ* XAFS analysis and so on, is needed to further strengthen the conclusion. In addition, the reaction mechanism of soot and CO oxidation over the developed catalyst should be investigated in future work.

STAR★METHODS

Detailed methods are provided in the online version of this paper and include the following:

- KEY RESOURCES TABLE
- RESOURCE AVAILABILITY
  - Lead contact
  - Materials availability
  - Data and code availability
- METHOD DETAILS
  - Catalyst preparations
  - Characterizations of the catalysts
  - Catalytic activity measurements
- QUANTIFICATION AND STATISTICAL ANALYSIS

SUPPLEMENTAL INFORMATION

Supplemental information can be found online at https://doi.org/10.1016/j.isci.2022.104103.

ACKNOWLEDGMENTS

This work was supported by the National Natural Science Foundation of China (51822811, 51908532), the Strategic Priority Research Program of the Chinese Academy of Sciences (XDA23010201), and the Science and Technology Innovation "2025" major program in Ningbo (2020Z103).

AUTHOR CONTRIBUTIONS

M. Wang: Investigation, Formal analysis, Writing-Original Draft, Review and Editing; Y. Zhang: Formal analysis, Data Curation, Supervision, Writing-Review and Editing, Project administration; W. Shan: Formal analysis, Supervision, Writing-Review and Editing, Project administration, Funding acquisition; Y. Yu: Data Curation, Writing - Review and Editing; J. Liu: Formal analysis, Review and Editing; H. He: Resources, Supervision, Funding acquisition.

DECLARATION OF INTERESTS

The authors declare no competing interests.

Received: November 17, 2021
Revised: February 9, 2022
Accepted: March 15, 2022
Published: April 15, 2022

REFERENCES

Atribak, I., Bueno-López, A., and García-García, A. (2008). Thermally stable ceria–zirconia catalysts for soot oxidation by O_2. Catal. Commun. *9*, 250–255.

Chang, H., Chen, X., Li, J., Ma, L., Wang, C., Liu, C., Schwank, J.W., and Hao, J. (2013). Improvement of activity and SO_2 tolerance of Sn-modified MnO_x-CeO_2 catalysts for NH_3-SCR at low temperatures. Environ. Sci. Technol. *47*, 5294–5301.

Cui, B., Zhou, L., Li, K., Liu, Y.Q., Wang, D., Ye, Y., and Li, S. (2020). Holey Co-Ce oxide nanosheets as a highly efficient catalyst for diesel soot combustion. Appl. Catal. B-Environ. *267*, 118670.

Farrauto, R.J., Deeba, M., and Alerasool, S. (2019). Gasoline automobile catalysis and its historical journey to cleaner air. Nat. Catal. *2*, 603–613.

Guo, Z., and Zhang, Z. (2007). Hybrid modeling and simulation of multidimensional processes for diesel particulate filter during loading and regeneration. Numer. Heat Tr. A-Appl. *51*, 519.

He, H., Lin, X., Li, S., Wu, Z., Gao, J., Wu, J., Wen, W., Ye, D., and Fu, M. (2018). The key surface species and oxygen vacancies in MnO_x(0.4)-CeO_2 toward repeated soot oxidation. Appl. Catal. B-Environ. *223*, 134–142.

Liu, C., Xian, H., Jiang, Z., Wang, L., Zhang, J., Zheng, L., Tan, Y., and Li, X. (2015). Insight into the improvement effect of the Ce doping into the SnO_2 catalyst for the catalytic combustion of methane. Appl. Catal. B-Environ. *176-177*, 542–552.

Liu, J., He, G., Shan, W., Yu, Y., Huo, Y., Zhang, Y., Wang, M., Yu, R., Liu, S., and He, H. (2021). Introducing tin to develop ternary metal oxides with excellent hydrothermal stability for NH3 selective catalytic reduction of NO. Appl. Catal. B-Environ. *291*, 120125.

Liu, W., Chen, Y., Qi, H., Zhang, L., Yan, W., Liu, X., Yang, X., Miao, S., Wang, W., Liu, C., et al. (2018). A durable nickel single-Atom catalyst for hydrogenation reactions and cellulose valorization under harsh conditions. Angew. Chem. Int. Ed. *57*, 7071–7075.

Liu, X., Zhou, K., Wang, L., Wang, B., and Li, Y. (2009). Oxygen vacancy clusters promoting reducibility and activity of ceria nanorods. J. AM. Chem. Soc. *131*, 3140–3141.

Monte, R.D., Fornasiero, P., Desinan, S., Kašpar, J., Gatica, J.M., Calvino, J.J., and Fonda, E. (2004). Thermal stabilization of $Ce_xZr_{1-x}O_2$ oxygen storage promoters by addition of Al_2O_3: effect of thermal aging on textural, structural, and morphological properties. Chem. Mater. *16*, 4273.

Mukherjee, D., Devaiah, D., Venkataswamy, P., Vinodkumar, T., Smirniotis, P.G., and Reddy, B.M. (2018). Superior catalytic performance of a CoO_x/Sn–CeO_2 hybrid material for catalytic diesel soot oxidation. New J. Chem. *42*, 14149–14156.

Ren, W., Ding, T., Yang, Y., Xing, L., Cheng, Q., Zhao, D., Zhang, Z., Li, Q., Zhang, J., Zheng, L., et al. (2019). Identifying oxygen activation/oxidation sites for efficient soot combustion over silver catalysts interacted with nanoflower-like hydrotalcite-derived CoAlO metal oxides. ACS Catal. *9*, 8772–8784.

Rodriguez-Carvajal, J. (1993). Recent advances in magnetic structure determination by neutron powder diffraction. Physica B *192*, 55–69.

Sasikala, R., Gupta, N.M., and Kulshreshtha, S.K. (2001). Temperature-programmed reduction and CO oxidation studies over Ce–Sn mixed oxides. Catal. Lett. *71*, 69–73.

Sellers-Anton, B., Bailon-Garcia, E., Cardenas-Arenas, A., Davo-Quinonero, A., Lozano-Castello, D., and Bueno-Lopez, A. (2020). Enhancement of the generation and transfer of active oxygen in Ni/CeO_2 catalysts for soot combustion by controlling the Ni-ceria contact and the three-dimensional structure. Environ. Sci. Technol. *54*, 2439–2447.

Venkataswamy, P., Rao, K.N., Jampaiah, D., and Reddy, B.M. (2015). Nanostructured manganese doped ceria solid solutions for CO oxidation at lower temperatures. Appl. Catal. B-Environ. *162*, 122–132.

Wang, B., Zhang, H., Xu, W., Li, X., Wang, W., Zhang, L., Li, Y., Peng, Z., Yang, F., and Liu, Z. (2020). Nature of active sites on Cu–CeO_2 catalysts activated by high-temperature thermal aging. ACS Catal. *10*, 12385–12392.

Wang, H., Luo, S., Zhang, M., Liu, W., Wu, X., and Liu, S. (2018). Roles of oxygen vacancy and O_x^- in oxidation reactions over CeO_2 and Ag/CeO_2 nanorod model catalysts. J. Catal. *368*, 365–378.

Wu, X., Liu, S., Weng, D., Lin, F., and Ran, R. (2011). MnO_x-CeO_2-Al_2O_3 mixed oxides for soot oxidation: activity and thermal stability. J. Hazard. Mater. *187*, 283–290.

Xu, H., Zhang, Z., Liu, J., Do-Thanh, C.L., Chen, H., Xu, S., Lin, Q., Jiao, Y., Wang, J., Wang, Y., et al. (2020). Entropy-stabilized single-atom Pd catalysts via high-entropy fluorite oxide supports. Nat. Commun. *11*, 3908.

Xu, L., Liang, H.W., Yang, Y., and Yu, S.H. (2018). Stability and Reactivity: positive and negative aspects for nanoparticle processing. Chem. Rev. *118*, 3209–3250.

Yan, D., Chen, J., and Jia, H. (2020). Temperature-induced structure reconstruction to prepare a thermally stable single-atom platinum catalyst. Angew. Chem. Int. Ed. *59*, 13562–13567.

Yang, X., Li, Q., Lu, E., Wang, Z., Gong, X., Yu, Z., Guo, Y., Wang, L., Guo, Y., Zhan, W., et al. (2019). Taming the stability of Pd active phases through a compartmentalizing strategy. Nat. Commun. *10*, 1611.

Yu, M., Luss, D., and Balakotaiah, V. (2013a). Regeneration modes and peak temperatures in a diesel particulate filter. Chem. Eng. J. *232*, 541.

Yu, M., Luss, D., and Balakotaiah, V. (2013b). Analysis of flow distribution and heat transfer in a diesel particulate filter. Chem. Eng. J. *226*, 68.

Zhang, Z., Zhu, Y., Asakura, H., Zhang, B., Zhang, J., Zhou, M., Han, Y., Tanaka, T., Wang, A., Zhang, T., and Yan, N. (2017). Thermally stable single atom Pt/m-Al_2O_3 for selective hydrogenation and CO oxidation. Nat. Commun. *8*, 16100.

Zhao, M., Deng, J., Liu, J., Li, Y., Liu, J., Duan, Z., Xiong, J., Zhao, Z., Wei, Y., Song, W., and Sun, Y. (2019). Roles of surface-active oxygen species on 3DOM cobalt-based spinel catalysts $M_xCo_{3-x}O_4$ (M = Zn and Ni) for NO_x -assisted soot oxidation. ACS Catal. *9*, 7548–7567.

STAR★METHODS

KEY RESOURCES TABLE

REAGENT or RESOURCE	SOURCE	IDENTIFIER
Chemicals, peptides, and recombinant proteins		
Ce(NO3)3·6H2O	Tianjin Fuchen Chemical Reagent Factory	CAS 10294-41-4
$SnCl_4 \cdot 5H_2O$	Shanghai Aladdin Biochemical Technology Co., Ltd	CAS 10026-06-9
$Co(NO_3)_2 \cdot 6H_2O$	Sinopharm Chemical Reagent Co., Ltd	CAS 10026-22-9

RESOURCE AVAILABILITY

Lead contact

Further information and requests for resources should be directed to and will be fulfilled by the lead contact, Wenpo Shan (wpshan@iue.ac.cn)

Materials availability

Materials generated in this study will be made available on reasonable request, but we may require a payment or a completed Materials Transfer Agreement if there is potential for commercial application.

Data and code availability

Data reported in this paper will be shared by the lead contact upon reasonable request.

This study does not report original code.

Any additional information required to reanalyze the data reported in this paper is available from the Lead Contact upon reasonable request.

METHOD DETAILS

Catalyst preparations

The catalyst was synthesized by a co-precipitation method. $Ce(NO_3)_3 \cdot 6H_2O$ and $SnCl_4 \cdot 5H_2O$, with different Ce/Sn molar ratios (Ce : Sn=3:1 of 6 g $Ce(NO_3)_3 \cdot 6H_2O$ and 1.61 g $SnCl_4 \cdot 5H_2O$, Ce : Sn=1:1 of 6 g $Ce(NO_3)_3 \cdot 6H_2O$ and 4.85 g $SnCl_4 \cdot 5H_2O$, Ce : Sn=1:3 of 2.49 g $Ce(NO_3)_3 \cdot 6H_2O$ and 6 g $SnCl_4 \cdot 5H_2O$), were dissolved together in deionized water. Then the above aqueous solution was added dropwise into another mixed solution consisting of H_2O : $NH_3 \cdot H_2O$: H_2O_2 = 4:4:1 (H_2O=80 ml, $NH_3 \cdot H_2O$=80 ml, and H_2O_2=20 ml) under vigorous mixing. Next, the obtained suspension was ultrasonicated for 30 minutes, stirred for 1 hour, and washed to neutral pH. The as-prepared precipitate was dried at 110°C for 12 h, and then calcined at 700°C for 3 h in air. The catalysts were named as $Ce_xSn_{1-x}O_2$, which did not mean the Ce and Sn species existing as CeO_2-SnO_2 solid solution. CeO_2 and SnO_2 were also synthesized using the same method as reference samples.

Three different theoretical Co loadings, 1%, 3% and 5% with regards to the weight of the support (2 g), were used to investigate the effect of Co loading on the oxidation reaction. Co loading was performed via wetness impregnation with appropriate amounts of an aqueous solution of $Co(NO_3)_2 \cdot 6H_2O$ (0.099 g $Co(NO_3)_2 \cdot 6H_2O$ of 1%, 0.296 g $Co(NO_3)_2 \cdot 6H_2O$ of 3%Co, and 0.494 g $Co(NO_3)_2 \cdot 6H_2O$ of 5%). The obtained mixture was ultrasonicated for 30 minutes and stirred for 1 h. Then, the mixture was subjected to a rotary evaporation process to remove water. Finally, the obtained powders were dried at 110°C overnight, then the powders were calcined at 700°C for 3 h in air. For comparison, the 3%Co/CeO_2 catalyst was synthesized using the same methods as above. The obtained catalysts were named as 1%Co/$Ce_{0.5}Sn_{0.5}O_2$, 3%Co/$Ce_{0.5}Sn_{0.5}O_2$, 5%Co/$Ce_{0.5}Sn_{0.5}O_2$, and 3%Co/CeO_2, respectively. In addition, the 3%Co/$Ce_{0.5}Sn_{0.5}O_2$ and 3%Co/CeO_2 catalysts were also calcined at 500, 900, and 1000°C for 3 h, respectively, for the thermal stability tests.

Characterizations of the catalysts

The X-ray diffraction (XRD) patterns were obtained on an X'Pert PRO instrument with Cu K_α radiation (λ= 1.5418) at 40 kV and 40 mA. Data were collected between 2θ=10-90°, with a scan step of 0.07°.

The Brunauer-Emmett-Teller (BET) method was applied to measure the specific surface areas of the samples via N_2 adsorption-desorption isotherms at − 196°C using an ASAP 2020N autoscore surface analyzer. The pore volume and pore-size were obtained by the BJH method using the desorption branch.

The morphologies and element mapping of the as-prepared catalysts were obtained with a high-resolution transmission Tecnai FEI-F20 electron microscope.

X-ray photo electron spectroscopy (XPS) results of the catalysts were obtained on a scanning X-ray micro probe (ESCALAB250I, Thermo Fisher scientific) using Al K α radiation. All of the binding energies were calibrated using the C 1s peak (BE = 284.8 eV) as standard.

H_2-TPR was performed using a Micromeritics Auto Chem II 2920 automatic chemical adsorption analyzer. After pre-treatment under 5% O_2 balanced by He at 500°C for 1 h, the 100 mg sample was heated from room temperature to 900°C at a constant rate (10°C/min) in a U-shaped quartz reactor under 10% H_2/Ar mixture gas (30 ml/min). The hydrogen consumption was monitored with a TCD detector, which was calibrated by the signal generated by the introduction of the known amounts of hydrogen.

Catalytic activity measurements

Printex-U (Degussa) was used as model soot, with particle size and specific surface area of 25 nm and 100 m^2/g, respectively. The catalytic activity was evaluated by a temperature programmed oxidation reaction, which was carried out in a continuous flow fixed bed reactor consisting of a quartz tube with 5 mm inner diameter. To make evaluation conditions close to actual practice, the loose contact was employed. Under the loose contact, the catalyst and soot were mixed for 2 minutes with a spatula. The mass ratio of catalyst to soot was 10:1, then 110 mg of the admixture was added to 300 mg of quartz sand with particle size from 40 to 60 mesh, in order to reduce air resistance and guard against reaction run off.

The reaction gas, including 1000 ppm NO (when used), 50 ppm SO_2 (when used), 10% O_2, and 5% H_2O (when used), with N_2 as balanced gas, was flowed into the fixed bed reactor at a total flow rate of 500 ml/min. The reaction temperature was increased from room temperature to 700°C at a heating rate of 10°C/min, which was measured by a K-type thermocouple in the fixed bed reactor. The outlet gases in the soot catalytic oxidation process, such as CO_2, CO, NO and NO_2, were detected by an Antaris IGS (Thermo Fisher) equipped with a heated, low-volume multiple-path gas cell (2 m).

Soot conversion and CO_2 selectivity were calculated as follows:

$$\text{Soot Conversion} = \frac{A_i}{A_t} \times 100\% \qquad \text{(Equation 1)}$$

The catalytic activity was described by the values of T_{10}, T_{50}, and T_{90}, which were defined as the temperatures at 10%, 50%, and 90% soot conversion, respectively.

$$CO_2\ \text{Selectivity} = \frac{A_{iCO_2}}{A_{iCO_2} + A_{iCO}} \times 100\% \qquad \text{(Equation 2)}$$

A_i is the total peak areas of CO_2 and CO at a given temperature, A_t is the total peak areas of CO_2 and CO overall, A_{iCO2} is the total peak area of CO_2 at a given temperature, and A_{iCO} is the total peak area of CO at a given temperature.

The CO oxidation activities for the prepared catalysts were also evaluated in a continuous flow fixed bed reactor using 100 mg catalysts in a gas mixture of 0.4% CO/10%O_2/N_2 at a flow rate of 500 ml/min. The reaction temperature was increased from room temperature to 700°C at a heating rate of 10°C/min, which was measured by a K-type thermocouple in the fixed bed reactor. The outlet gases, such as CO_2 and CO, were detected by an Antaris IGS (Thermo Fisher) equipped with a heated, low-volume multiple-path gas cell (2 m).

CO conversion was calculated as follows:

$$CO\ \text{Conversion} = \frac{CO_{in} - CO_{out}}{CO_{in}} \times 100\% \qquad \text{(Equation 3)}$$

QUANTIFICATION AND STATISTICAL ANALYSIS

Our study doesn't include quantification and statistical analysis.